Friction power modeling and measurements in sliding vane rotary compressors

Giuseppe Bianchi, Roberto Cipollone*

Department of Industrial and Information Engineering and Economics, University of L'Aquila, Via Giovanni Gronchi 18, 67100 L'Aquila, Italy

Abstract

In compressed air systems, mechanical and organic losses account for 15 % of compressor energy consumption. In the current research, the energy saving potential achievable through friction power reduction in sliding vane rotary compressors was investigated using experimental and modeling approaches. Tests on a new mid-size industrial compressor operating at different steady conditions (outlet pressure 9, 12.5, 14.5 bar at 1000 and 1500 RPM) assessed the machine performance through measurement of mechanical power and the reconstruction of the pressure-volume diagram. An experimental methodology was also developed to quantify the power lost by friction and its measurement uncertainty using the concept of indicated mean effective pressure. Modeling the compressor blade dynamics allowed a friction power decomposition while an analysis of the hydrodynamic lubrication at the most severe friction location, namely between blade tip and stator wall, additionally provided the oil film thickness evolution along the contact surface. The agreement between modeling and experimental data identified a value for the friction coefficient of 0.065. Design suggestions on existing machines and new design solutions were eventually outlined varying blade mass, revolution speed and compressor aspect ratio. These improved configurations predicted an efficiency increase up to 6 %.

Keywords: sliding vane rotary compressor, compressed air systems, indicator diagram, friction, mechanical efficiency, piezoelectric pressure transducer

1. Introduction

Compressed air is an indispensable utility for most of the industrial processes since it allows productivity gains and work reduction in a safe way. However, from energetic and economic viewpoints, its production is an expensive and inefficient process. Indeed, most of the life cycle costs of an industrial Compressed Air System (CAS) are the energy costs [1]. For this reason, CAS are responsible of 10 % of electricity

*Corresponding author

Email addresses: giuseppe.bianchi@graduate.univaq.it (Giuseppe Bianchi), roberto.cipollone@univaq.it (Roberto Cipollone)

consumptions in EU-15 European countries, 9.4 % in China and about 10 % of the global industrial energy use in the United States [2]. Recent studies state that the saving potential in industrial CAS ranges from 20 % to 50 % [3]. Hence, around 400 TWh/yr of primary energy could be saved.

Nowadays, the most widespread industrial compression technology is the rotary volumetric one since it allows to cover a wide range of flow rates and delivery pressures. To address the short term efficiency improvements in the rotary compression technology, reference to the database of the Compressed Air and Gas Institute (CAGI) was made [4]. A normalization procedure was developed to compare different technologies (mainly screw and sliding vane) relying on performance datasheets provided by the compressors manufacturers [5]. In order to estimate the minimum energy saving achievable, only best machines currently in the market (i.e. those with the minimum energy requirement for any compression ratio) were considered. Figure 1 reports the specific electric consumptions (E_{el}) at different delivery pressures: an asymptotic trend with increasing flow rate can be noticed. Hence, premium machines are usually big size compressors.

[Figure 1 about here.]

Performance data closely match the trend depicted with solid line, whose calculation was performed according to Equation 1 and a global efficiency of 80 %:

$$E_{el} = \frac{1}{\eta_{glob}} \frac{k\, R\, T_{inl}}{k-1} \left(\beta^{\frac{k-1}{k}} - 1 \right) \tag{1}$$

The global efficiency η_{glob} takes into account several contributions that are expressed through Equation 2.

$$\eta_{glob} = \eta_{el}\, \eta_{mech}\, \eta_{org}\, \eta_{vol}\, \eta_{ad-is} \tag{2}$$

The saving potential achievable in rotary volumetric compressors has been outlined following two approaches related to mechanical improvements or both mechanical and thermodynamic improvements. The lowest specific energy consumptions might be attained if the compression transformation moved from the current adiabatic trend to an isothermal one (dash-dot line): in this case the numerator of Equation 1 would become $R\,T_{inl}\, ln(\beta)$. Although a pure isothermal compression can not be reached, it might be approached using multiple inter-cooled stages or through an internal air cooling. The latter strategy has been pursued by means of modeling [6] and testing [7, 8] activities relying on the cooling capabilities of the compressor lubricant when sprayed in the compressor vanes [9].

With reference to an adiabatic compression process ($\eta_{ad-is} \approx 1$), the distance between solid and dashed lines in Figure 1 represents the energy saving potential that exists between the state of the art ($\eta_{glob} \approx 80\%$) and the ideal compressor performance (dashed line). When considering premium machines as the one plotted in Figure 1, electrical and volumetric losses are negligible since those compressors were properly designed and equipped with high-efficiency motors. Therefore, the saving potential is only due to mechanical and organic improvements of the compressor. On the other hand, when considering also a different compression transformation, mechanical and organic improvements accounts as the half of the overall saving potential.

The literature related to Sliding Vane Rotary Compressors (SVRCs) is not as extensive as the one for other compression technologies. The state of the art and future perspectives in the sliding vane technology were recently reviewed by Cipollone [10]. Available research papers mainly focus on models that describe single or multiple phenomena occurring in these machines [11, 12]. Previous experimental works additionally provided methodologies to evaluate the compressor machine using different measurement techniques such as the hot by pass calorimeter or the more sophisticated indicator diagram both for compressors [13, 14] and expanders [15, 16, 17]. As concerns friction losses in SVRCs, they were investigated mainly through theoretical studies. Badr et al. provided an extensive mathematical model for friction losses in rotary vane machines. They analyzed both circular and non-circular machines concluding that blade dynamics is the most affecting phenomenon for friction. In particular, the most critical friction location identified was the one between the blade tip and stator wall [18]. Indeed, the contributions at shaft bearings or between rotor and end wall plates revealed negligible compared to the power dissipated between the compressor blades with rotor and stator because of the absence of axial loads. Thus, most of the research focused on the blade dynamics using geometrical approaches and solving the Newton's 2nd law of motion. Aradau et al. proposed a model in which the effects of the Coriolis force were also taken into account. They suggested an abundant lubrication and blade tilting to lower friction [19]. The latter strategy was also investigated by Tramschek and Mkumba. However, they concluded that the benefits achievable with a forward blade tilt do not justify an increased cost of the machine [20]. Platts coupled the study of the blade dynamics to the analysis of the hydrodynamic lubrication at blade tip. Design suggestions related to surface roughness and corresponding lubrication regime established were provided [21]. Lindemann et al. performed measurements and optimizations on the blade tip radius concluding that this parameter should be at least the half of the vane thickness but not greater than then stator curvature for any rotor position. Otherwise no uniform curvature would be achieved [22].

Unlike the above mentioned research that mainly focused on single features of sliding vane compressors, the current paper provides a comprehensive approach: all the fundamental processes that affect the compressor energy consumption were taken into account and simulated at the same time to reduce the number of assumptions to be made. Furthermore, since the model is fully parameterized, analyses can be performed on any compressor layout to understand the limits of existing configurations and to address future improved designs. As concerns the experimental activity, the paper introduces a methodology to assess the measurement uncertainty on the reconstruction of the indicator diagram that is the most important tool to understand the compressor behavior. The paper shows the reconstruction procedure, energy breakdown at different operating points and how the measurement uncertainty propagated within each contribution. As the model was calibrated through an experimental campaign on a mid-size industrial sliding vane compressor, a friction power decomposition was carried out to identify the most affecting parameters. Improvements on existing and new design solutions were eventually outlined.

2. Friction power mathematical model

The main processes occurring in a SVRC were modeled through a comprehensive approach [23] whose sub-modules are summarized in Figure 2. The model is able to represent:

[Figure 2 about here.]

- compressor geometry for any machine layout: axial or radial intake and exhaust ports, radial or tilted blades, circular or elliptical stators;
- flow dynamics during vane filling and emptying processes using an unsteady one-dimensional formulation along the pipes connected to the compressor cells. The vane behaved as plenum of finite capacity and acted as boundary condition for the mass and momentum equations whose solutions were calculated using the quasi-propagatory model (QPM) [24]. QPM is particularly suitable to investigate the main properties of 1D transient flows since it provides accurate results at a lower computational cost compared to other approaches as the method of characteristics [25];
- cell pressure evolution during the compression phase (i.e. from the end of vane filling to the beginning of the compressed air discharge). The knowledge of the vane geometry and the application of the unsteady energy equation (in lumped form) eventually allowed to evaluate the compression work, and heat exchanges according to the approach proposed by Tan and Ooi [26];
- lubrication circuit with oil injection and separation before the air delivery to the compressed air line;

The blade dynamics was modeled with reference to the Newton's 2nd law of motion. Since the blade has a translational motion (entrance and exit from rotor slots) combined to rotation, fictitious forces act on it (centrifugal and Coriolis ones). Furthermore, as reported in Figure 3.a, during the compression phase the pressure difference across two adjacent cells tends to tilt the blade backward.

[Figure 3 about here.]

The set of equations which regulates the translational (2 directions) and rotational equilibria are reported, in a matrix form, in Equation 3: forces are projected through the coefficients ζ_{1-4} with respect to the blade slot axis. The unknowns are forces exchanged at the friction locations, namely at the blade tip and with the side walls of the rotor slot. Depending on the signs of F_1 and F_2 with respect to Figure 3.a, the blade may assume the arrangements depicted in Figure 3.b.

$$\begin{pmatrix} 1 & -1 & -\zeta_2 \\ -\lambda & -\lambda & \zeta_1 \\ 0 & \lambda\, t_{bl} - (L_{bl} - L_{os}) & \zeta_2\, L_{os} - \zeta_1\, t_{bl}/2 \\ & & \end{pmatrix} \begin{pmatrix} F_1 \\ F_2 \\ F_3 \\ \end{pmatrix} =$$

$$\begin{pmatrix} F_{pn} - F_{cor} + \zeta_4\, F_{cen} \\ F_{in} + \zeta_3\, F_{cen} \\ F_{cen}(\zeta_4\,(L_{bl}/2 - L_{os}) - \zeta_3\, t_{bl}/2) ... \\ ... - F_{pn}\, L_{os}/2 - F_{in}\, t_{bl}/2 - F_{cor}(L_{bl}/2 - L_{os}) \end{pmatrix} \tag{3}$$

Once F_1, F_2 and F_3 are known, overall friction power is calculated as:

$$P_{fr} = \lambda(F_3\, U + v_{bl}(F_1 + F_2)) \tag{4}$$

where U is the peripheral tip speed and v_{bl} the blade slip velocity with respect to the rotor slot. The friction coefficient λ in Equation 4 was identified through the experimental procedure explained in Section 3.

A noteworthy aspect that plays a key role in the overall friction power dissipation is the lubrication regime between blade tip and stator wall. The oil pressure distribution must continuously balance the varying load at blade tip ($\zeta_1\, F_3$). Furthermore, minimum thickness of the oil layer must be seriously taken under control to avoid dry contacts. In order to assess these issues, the hydrodynamic behavior of the blade tip sliding on the oil layer which stands at the stator surface was additionally studied. As reasonably occurs in the middle cross section of the compressor, assuming that lubrication conditions do not vary along the axial length of the blade-stator contact, a one-dimensional approach was used: at any angular position of the blade θ, Equation 5 combined the tip blade geometry (circular arc) and the Reynolds equation to calculate pressure distribution along the contact between blade tip and stator, whose local coordinate is indicated with ξ and shown in Figure 3.c.

$$\frac{d}{d\xi}\left(\frac{h(\xi)^3}{12\mu}\,\frac{dp(\theta)}{d\xi}\right) = \frac{u_{oil}(\xi)}{2}\,\frac{dh(\xi)}{d\xi} \tag{5}$$

The location at which the pressure distribution is maximum ($dp/d\xi$=0) simplifies Equation 5 and allows the analytical calculation of the oil film thickness in this particular case according to Equation 6.

$$h_0(\theta) = \frac{\int_0^{t_{bl}} h^{-2}(\xi, \theta)\, d\xi - (p_{LV}(\theta) - p_{TV}(\theta))/(6\,\mu\, u_{oil}(\theta))}{\int_0^{t_{bl}} h^{-3}(\xi, \theta)\, d\xi} \tag{6}$$

Elsewhere, the mathematical problem for the hydrodynamic lubrication at the blade tip does not have an explicit solution. Hence, based on the methodology proposed by Fowell et al. [27], Equation 5 was linearized and discretized: at a given node of the spatial domain, the oil flow rate per unit surface q_j was modeled according to Equation 7.

$$q_j = \frac{u_{oil}\, h_j}{2} - \frac{{h_j}^3}{12\mu} \frac{p_{j+1} - p_j}{\Delta\xi} \tag{7}$$

where the values of the film thickness h are the sum of h_0 and the gap between stator wall and blade tip profile, known from the compressor geometry. The mass conservation within flow elements separated by two consecutive nodes ($q_{j-1} = q_j$, for $j = 1$ to $n-1$) led to a system of $n-1$ equations that were solved to find the unknown pressures p_j. Pressure values in the leading ($j = 0$) and trailing ($j = n$) compression chambers separated by the blade were boundary conditions for the problem provided by the thermodynamic cell module of the compressor model (Figure 2). If infinite pressure gradients occur, the film thickness becomes discontinuous and reveals a dry contact between stator and blade, thus a sudden increase of friction dissipations as well as structural damages for compressor.

3. Experimental Activity

In a sliding vane compressor, friction occurs at several locations of the machine: shaft bushes, end wall plates, blade tip and side walls, etc. Even though there are studies in which the first two terms revealed negligible compared to the other ones [18], an accurate experimental methodology would require separate evaluations. Furthermore, all the above mentioned locations are characterized by the presence of a lubricating medium that mitigates friction between components in relative motion. However, all the lubricant paths refer to a unique oil circuit driven by a pressure difference proportional to exhaust and intake values. After separation from air, the oil is recycled in a tank at a temperature higher than the injection one. This enthalpy gain, further dissipated through a radiator to preserve the lubricating properties of the oil, cannot exclusively be attributed to the power lost by friction. Indeed, it also takes into account the heat exchange with air and the metallic surfaces of the compressor. For these reasons, a direct experimental evaluation of the friction power is not achievable.

3.1. Experimental Methodology

Out of all the mechanical power supplied to a sliding vane compressor, only part of it goes to accomplish the compression process; the remaining contributions account for oil pressurization and mechanical losses, as stated in Equation 8:

$$P_{fr} = P_{mech} - P_{ind} - P_{oil} \tag{8}$$

The right-hand side of the energy balance contains quantities that can be directly measured and leads to the friction losses evaluation in an indirect way.

To estimate the friction coefficient λ in Equation 4, this experimental methodology was applied on a novel mid-size industrial sliding vane compressor (Mattei ERC 22 L) whose geometrical features are listed in Table 1.

[Table 1 about here.]

Figure 4 shows the layout and sensors types: low frequency pressure transducers and thermocouples were installed in relevant points of the machine while a gear flow meter and an ISA 1392 nozzle provided the oil and air mass flow rates measurements respectively. A flange torque meter was eventually used to measure the mechanical power as product of torque and revolution speed.

[Figure 4 about here.]

The knowledge of pressure and volume evolutions during vane rotation was a fundamental step to evaluate the compressor performance. Four piezoelectric transducers were circumferentially mounted on an end wall plate in order to give a continuous pressure monitoring (Figure 4). Since each of them provided a differential pressure with cyclic dispersion from one vane passage to the other, data were preliminary ensemble averaged over 10 acquisitions and further offset according to the pressure measurements at the intake and exhaust ports. The result of this intermediate processing is reported in Figure 5. Each pressure trace reports the uncertainty band due to the transducer (Kistler 601A).
The electric motor was directly connected to the compressor shaft. Hence, the magnetic incremental encoder installed on the motor (Figure 4) allowed to reference the pressure signals with respect to the crank angle. The knowledge of the cell volume evolution over a rotation cycle, provided by the geometrical section of the model, eventually led to the reconstruction of the indicator diagram and the calculation of the indicated power according to Equation 9.

$$P_{ind} = N\,\omega \oint p\,dV \tag{9}$$

The ratio between indicated and mechanical powers defines the mechanical compressor efficiency $\eta_{mech,SVRC}$.

$$\eta_{mech,SVRC} = P_{ind}/P_{mech} \tag{10}$$

The oil is injected inside the vanes through a set of plane orifices and its circulation is guaranteed by the compressor itself which pressurizes it through the air. The pressure loss during injection must be therefore restored. The pressurization power required was calculated according to Equation 11

$$P_{oil} = \frac{Q_{oil}\,\Delta p}{\eta_C} = \frac{Q_{oil}\,(p_{tank} - p(\theta_{inj}))}{\eta_{mech,SVRC}} \tag{11}$$

Friction power was eventually expressed as:

$$P_{fr} = C\,\omega - P_{ind} - C\,\omega\,\frac{Q_{oil}\,(p_{tank} - p(\theta_{inj}))}{P_{ind}} \tag{12}$$

3.2. Uncertainty Analysis

Since friction power was indirectly measured, its uncertainty resulted from the propagation of all the uncertainties related to the quantities directly measured according to Equation 13:

$$\left(\Delta P_{fr}\right)^2 = \sum_i \left(\frac{\partial P_{fr}}{\partial x_i} \, \Delta x_i \right)^2 \qquad x_i = C,\, \omega,\, P_{ind},\, Q_{oil},\, p_{tank},\, p(\theta_{inj}) \tag{13}$$

Direct measurements uncertainties are reported in Table 2. A noteworthy statement needs to be made on the uncertainty evaluation of the indicated power. To properly offset the differential pressure traces that led to the chart in Figure 5, the continuity on the first and second derivatives had to be preserved despite the sudden change in the signals due to the blade passage on the sensing elements. Furthermore, since all the piezoelectric transducers were the same, the sensor uncertainty (0.125 bar) had a relative value that increased if the differential pressure measured was low, as in sensors #1 and #4.

[Table 2 about here.]

[Figure 5 about here.]

In order to take into account these variations, the concept of indicated mean effective pressure (IMEP) was used to estimate the overall uncertainty on the indicated power. IMEP is the average pressure which, when multiplied by the vane swept volume, would require the same work out of the cycle as the real pressure, Equation 14.

$$IMEP = \frac{P_{ind}}{N \, \omega \, V_{swept}} = \frac{1}{V_{swept}} \oint p \, dV \tag{14}$$

For the test case at 1500 RPM and 12.5 bar, the value of IMEP is reported in Figure 5. Since the cell volume evaluation and revolution speed measurement were accurate, with reference to Equation 14, the only contribution which played an important role in the uncertainty of the indicated power was the value related to IMEP. Assuming that uncertainty on IMEP was the one of the piezoelectric pressure transducers, the resulting value on the indicated power was around 4 % (Table 3). This quantity had a strong influence on the uncertainty of the friction power computed as in Equation 13. Indeed, in absolute terms ΔP_{ind} is more than 25 % of the friction power. To reduce the magnitude of this contribution, a more accurate pressure measurement is needed. A step change in the accuracy of the indicating pressure measurement is under development using piezo-resistive pressure transducers whose spans decrease along the compression phase. This instrumentation will prevent to offset the pressure traces and to minimize the weight of the transducer uncertainty on the IMEP measurement.

3.3. Results

The industrial vane compressor was tested at different outlet pressures and revolution speeds. Table 3 summarizes the testing conditions, machine performance and the uncertainty of indicated and friction powers.

[Table 3 about here.]

Figure 6 shows a bar chart with the energy balance formulated in Equation 8. The indicated power increased with discharge pressure and revolution speed. Indeed, the first parameter acts on the area of the indicator diagram while the second one on the overall mass flow rate compressed. At 12.5 bar, the compressor efficiency ranged from 87 % at 1000 RPM to 86 % at 1500 RPM while the specific energy consumptions at ISO 1217 conditions (20°C, 1 bar) were 5.6 kW/(m^3/min) and 6 kW/(m^3/min), respectively. An unexpected result was the magnitude of power requested by the oil circulation that varied with discharge pressure but not with revolution speed. Even though the oil density with respect to the air one is almost three order of magnitudes higher, the power requested to fulfill the oil injection (Equation 11) accounted for up to 7 % of the shaft power. This is mainly due to the amount of oil flowing inside the machine. Therefore, a design suggestion would be to limit as much as possible the oil circulation without going below the minimum flow rate required for vane sealing and stable lubrication between components in relative motion. The amount of oil that exceeds this minimum threshold represents an energy waste. However, it's a common industrial practice to equip oil flooded compressor with an abundant amount of oil to extend the lubricant lifetime, so lowering maintenance costs.

[Figure 6 about here.]

Compressor speed influenced friction power since it acted both on centrifugal and Coriolis forces as well as all the slip velocities. Since the centrifugal force is proportional to the square of revolution speed and the peripheral tip speed is linearly dependent with ω, an overall cubic dependency could be stated between compressor speed and friction power. On the other hand, the discharge pressure did not have a relevant influence on friction power. This allowed to identify a unique value for the friction coefficient λ which was kept constant also at different revolution speeds. Minimizing the root mean square of the difference given by Equation 4 and the experimental data, a value of 0.065 was calculated. This value reproduced the power lost friction within the uncertainty band, as reported in Figure 7.

[Figure 7 about here.]

4. Friction power decomposition

After identifying a value for the friction coefficient, the relative magnitude of the terms in Equation 4 was calculated. Figure 8 shows the load distribution at friction locations over a whole revolution cycle. It is evident how F_3 (blade tip) and F_2 (at the bottom of the slot) remain almost unchanged during rotation, with F_3 almost always greater than F_2. This last term, for a great part of the rotation (during the intake and the first part of the compression phase) is close to zero; in the last portion of the compression process and during the discharge it increases till to 500 N. On the contrary, F_3 does not show significant variations from the mean value of 500 N. F_1 follows the same trend of F_2 but during the last part of the compression and discharge shows a sudden increase up to 3500 N. Indeed, when the first blade of the compressor cell reaches the exhaust port, the discharge pressure is suddenly imposed to the vane and increases the pressure force F_{pn} on the second blade of the cell (Figure 3.a). Hence, the load peak that F_1 balances is anticipated from the exhaust port opening of an angular extent equal to the vane width (360°/N). A higher discharge pressure (14.5 bar) contributes to increase the overall blade load but only for a limited angular extent, namely the discharge phase. This fact justifies the constancy of friction power at different discharge pressures and constant revolution speed that was noticed experimentally.

[Figure 8 about here.]

Figure 9 reports the comparison between normal load at blade tip ($\zeta_1 F_3$) and minimum thickness of the oil film resulting from Equation 5. An increase of the orthogonal load thins the oil layer between stator and blade tip. A sudden load increase occurs at 180° since the blade inverts its direction of motion. Hence, in the second half of the rotation cycle F_3 must not only balance the centrifugal force but also the blade inertia (as shown in the free body diagram of Figure 3.a). The lowest value of minimum thickness occurs in correspondence of the maximum load that is shifted before the exhaust port opening by a quantity equal to the angular width of the compression chamber. This trend is in agreement with the one reported in Figure 8. The lubrication never exceeds the hydrodynamic regime. Therefore, SVRCs ensure vane sealing without any risk of dry contact that would highly affect the energy expenditure due to friction losses.

[Figure 9 about here.]

To calculate the instantaneous friction power, the knowledge of slip speeds was required: in the compressor tested, at 1500 RPM the peripheral tip speed U had a mean value of 0.6 m/s while the sliding velocity with respect to the rotor slot v_{bl} had a sinusoidal trend since the blade enters and exits from the slot each revolution cycle: mean velocity was 0.08 m/s with an amplitude of 0.65 m/s. The product of reaction forces and sliding speeds along the whole revolution cycle led to the friction power decomposition displayed in Figure 10. Although the maximum blade load occurs at the top of the rotor slot during the discharge phase, the most affecting contribution to the overall friction loss is the one at the blade tip because of the higher order of magnitude the corresponding slip velocity. In terms of mean values, friction at the blade tip accounts for 80 % of the overall dissipation while the ones related to F_1 and F_2 are responsible for the 16 % and 4 % respectively.

[Figure 10 about here.]

5. Design Suggestions

Model predictions were applied on existing compressors to address short-term efficiency improvements. Furthermore, high-efficiency design configurations were outlined investigating the roles of revolution speed and blade mass on the overall friction power dissipated.

Figure 11 shows the effect of blade mass on the specific friction power (i.e. friction power per unit air at ISO 1217 conditions) at different compressor speeds. Blade weight reduction might be performed either removing some material from the component or replacing the current blade material (cast iron) with a lighter one, provided that compatibility from the mechanical (structural integrity) and tribology (lubrication and wear) viewpoints are still ensured. Keeping the same geometry, each point of the curves in Figure 11 simulates a machine in which volumetric flow rate decreased if revolution speed was lower than the reference test case (1500 RPM at 12.5 bar). Considering that nominal speed of current industrial sliding vane compressors is usually 1500 RPM, the reduction to 1000 RPM would decrease the effects of friction from 0.78 $kW/(m^3/min)$ to 0.44 $kW/(m^3/min)$. Mass reduction is also effective on friction power reduction: at 1500 RPM, a 60 % decrease of the blade mass would produce a 52 % saving while a blade 80 % lighter than the conventional one would lead to a saving of 61 %. However, potential drawbacks of lowering the blade inertia could be oil film instability (dry contacts) as well as a significant change in the dynamic effects that could alter the vane sealing, thus the volumetric efficiency of the machine.

[Figure 11 about here.]

Figure 12 shows two sets of curves at constant flow rate. To restore the reference value (test case at 1500 RPM, 12.5 bar), the axial length variation had to be inversely proportional to the compressor speed change. For instance, at 1000 RPM the compressor was one third longer. In these conditions, two design solutions for the blades inertia were explored: constant linear mass or constant mass. The first approach (constant linear mass - solid lines) required a blade mass variation proportional to the axial length. The centrifugal force has a quadratic dependency with the revolution speed but is also proportional to the blade mass. On the other hand, the inertia force is linearly influenced both by the revolution speed and the blade mass. Therefore, the opposite variation of blade mass with respect to the change of revolution speed decreases the friction power reduction that could be achieved. This constraint is overcome by the second approach (constant mass - dashed lines) that keeps the same blade mass of the reference test case. In this way, the effects of mass and speed reduction combine to produce a greater friction power reduction: using the current blade material, at 1000 RPM the constant linear mass approach would decrease specific friction power up to 0.45 $kW/(m^3/min)$ while the constant mass one would lead to 0.37 $kW/(m^3/min)$.

[Figure 12 about here.]

The knowledge acquired with the experimental activity and the simulations allows to outline the following suggestions to design a high-efficiency sliding vane rotary compressor:

- lowering the revolution speed has relevant benefits on the friction power reduction without compromising the volumetric efficiency of the machine. This fact does not apply to other rotary compression technologies;
- even though the maximum blade load does not occur at the blade tip, this location is the main contribution to friction loss because of the magnitude of the slip speed. Therefore, to restore the volumetric capacity of the machine lowered by the revolution speed reduction, the geometry of the compressor can be modified increasing the axial length of the compressor rather than the stator diameter;
- friction losses can be reduced decreasing the blade mass. Weight reductions can be achieved either through a suitable removal of some material from existing blades or using a lighter material.

An additional geometrical parameter, represented by the blade tilt with respect to the radial direction, revealed very insensitive on the friction power. Indeed, tilting the blades slightly modified the load distribution but did not affect the slip velocities. Hence, the magnitude of the energy benefit predicted was hardly noticeable. This is in agreement with literature studies [20]. On the other hand, lowering the blade load through forces projection might allow to use materials with lower Young modulus that are usually also lighter than the current one.

6. Conclusions

The current research investigated the energy saving potential in sliding vane rotary compressors achievable through a friction power reduction. Unlike literature studies, the compressor was modeled with a comprehensive approach composed of dedicated modules interacting together. Among them, the study of blade dynamics and hydrodynamic lubrication at blade tip allowed a full friction power decomposition. The model was calibrated and validated by means of a test campaign on a new mid-size industrial sliding vane compressor operating at different outlet pressure levels and revolution speeds. Experiments revealed that friction accounts for 10 % of the mechanical power; this share increases at high revolution speeds but it is not remarkably affected by the outlet pressure. The measurement uncertainty concerned to the indirect evaluation of friction power pointed out the need to improve the indicating measurement technique. This goal could be achieved using absolute piezo-resistive transducers rather than piezo-electric ones. The experimental activity also allowed to identify a unique value of 0.065 for the friction coefficient of the compressor model. The simulation platform was eventually used to address improvements on existing machines and to outline design suggestions for future compressors acting on revolution speed, blade mass and compressor aspect ratio: reducing the operating speed from 1500 RPM to 1000 RPM would lead to a specific friction power reduction of 56 % while a blade 40 % lighter would further lower the specific friction power up to 0.28 $kW/(m^3/min)$.

Acknowledgement

The Authors acknowledge Ing. Enea Mattei S.p.A. and particularly its CEO, Dr. Giulio Contaldi, for continuous research funding and support. The work has been done also under the FP7 Project ”Complete Vehicle Energy-Saving CONVENIENT” founded by the European Commission.

References

[1] Carbon Trust, GPG385 energy efficient compressed air systems, `www.air-receivers.co.uk/files/Carbon_Trust_GPG385.pdf`, last access: 2014-05-13.

[2] R. Saidur, N. Rahim, M. Hasanuzzaman, A review on compressed-air energy use and energy savings, Renewable and Sustainable Energy Reviews 14 (4) (2010) 1135 – 1153. doi:10.1016/j.rser.2009.11.013.

[3] A. McKane, Improving energy efficiency of compressed air system based on system audit, Lawrence Berkeley National Laboratory.
URL `escholarship.org/uc/item/13w7f2fc`

[4] Compressed Air & Gas Institute, CAGI datasheets, `www.cagi.org/performance-verification/data-sheets.aspx`, last access: 2014-06-20.

[5] D. Vittorini, G. Bianchi, R. Cipollone, Energy saving potential in existing volumetric rotary compressors, Energy Procedia.

[6] R. Cipollone, G. Bianchi, G. Contaldi, Sliding vane rotary compressor energy optimization, in: ASME 2012 International Mechanical Engineering Congress and Exposition, American Society of Mechanical Engineers, 2012, pp. 69–80. doi:10.1115/IMECE2012-85955.

[7] G. Bianchi, R. Cipollone, S. Murgia, G. Contaldi, Development of an internal air cooling sprayed oil injection technique for the energy saving in sliding vane rotary compressors through theoretical and experimental methodologies, International Journal of Refrigerationdoi:10.1016/j.ijrefrig.2014.12.020.

[8] R. Cipollone, G. Valenti, G. Bianchi, S. Murgia, G. Contaldi, T. Calvi, Energy saving in sliding vane rotary compressors using pressure swirl oil atomizers, Proceedings of the Institution of Mechanical Engineers, Part E: Journal of Process Mechanical Engineeringdoi:10.1177/0954408914550356.

[9] G. Valenti, L. Colombo, S. Murgia, A. Lucchini, A. Sampietro, A. Capoferri, L. Araneo, Thermal effect of lubricating oil in positive-displacement air compressors, Applied Thermal Engineering 51 (12) (2013) 1055 – 1066. doi:10.1016/j.applthermaleng.2012.10.040.

[10] R. Cipollone, Sliding vane rotary compressor technology and energy saving, Proceedings of the Institution of Mechanical Engineers, Part E: Journal of Process Mechanical Engineeringdoi:10.1177/0954408914546146.

[11] R. Cipollone, G. Contaldi, A. Sciarretta, R. Tufano, C. Villante, A theoretical model and experimental validation of a sliding vane rotary compressor, in: Proceedings of the International Compressor Engineering Conference, no. 1755, Purdue University, 2006.
URL `docs.lib.purdue.edu/icec/1755/`

[12] O. Al-Hawaj, Theoretical modeling of sliding vane compressor with leakage, International Journal of Refrigeration 32 (7) (2009) 1555 – 1562. doi:10.1016/j.ijrefrig.2009.07.005.

[13] Y. M. Huang, S.-A. Yang, A measurement method for air pressures in compressor vane segments, Measurement 41 (8) (2008) 835 – 841. doi:10.1016/j.measurement.2005.11.027.

[14] Y. Teh, K. Ooi, Experimental study of the revolving vane (rv) compressor, Applied Thermal Engineering 29 (1415) (2009) 3235 – 3245. doi:10.1016/j.applthermaleng.2009.04.029.

[15] B. Yang, X. Peng, Z. He, B. Guo, Z. Xing, Experimental investigation on the internal working process of a co2 rotary vane expander, Applied Thermal Engineering 29 (1112) (2009) 2289 – 2296. doi:10.1016/j.applthermaleng.2008.11.023.

[16] C. Xia, W. Zhang, G. Bu, Z. Wang, P. Shu, Experimental study on a sliding vane expander in the hfc410a refrigeration system for energy recovery, Applied Thermal Engineering 59 (12) (2013) 559 – 567. doi:10.1016/j.applthermaleng.2013.05.050.

[17] R. Cipollone, G. Bianchi, D. D. Battista, G. Contaldi, S. Murgia, Mechanical energy recovery from low grade thermal energy sources, Energy Procedia 45 (0) (2014) 121 – 130. doi:10.1016/j.egypro.2014.01.014.

[18] O. Badr, S. Probert, P. O'Callaghan, Multi-vane expanders: Vane dynamics and friction losses, Applied Energy 20 (4) (1985) 253 – 285. doi:10.1016/0306-2619(85)90018-2.

[19] D. Aradau, L. Costiuc, Friction power in sliding vane type rotary compressors, in: Proceedings of the International Compressor Engineering Conference, no. 1357, Purdue University, 1996.
URL `docs.lib.purdue.edu/icec/1357/`

[20] A. Tramschek, M. Mkumbwa, Mathematical modelling of radial and non-radial rotary sliding vane compressors, in: Proceedings of the International Compressor Engineering Conference, no. 1151, Purdue University, 1996.
URL `docs.lib.purdue.edu/icec/1151/`

[21] H. Platts, Hydrodynamic lubrication of sliding vanes, in: Proceedings of the International Compressor Engineering Conference, no. 187, Purdue University, 1976.
URL `docs.lib.purdue.edu/icec/187/`

[22] H. Lindemann, H. Kaiser, M. Kuever, H. Kruse, Optimization of a special shaped rotary vane compressor-comparison of theoretical and experimental results, in: Proceedings of the International Compressor Engineering Conference, no. 393, Purdue University, 1982.
URL `docs.lib.purdue.edu/icec/393/`

[23] G. Bianchi, R. Cipollone, Theoretical modeling and experimental investigations for the improvement of the mechanical efficiency in sliding vane rotary compressors, Applied Energy 142 (2015) 95 – 107. doi:10.1016/j.apenergy.2014.12.055.

[24] R. Cipollone, A. Sciarretta, The quasi-propagatory model: A new approach for describing transient phenomena in engine manifolds, SAE Technical Paper (2001-01-0579). doi:10.4271/2001-01-0579.

[25] J. H. Horlock, D. Winterbone, The thermodynamics and gas dynamics of internal-combustion engines, Oxford University Press, 1986.

[26] K. Tan, K. Ooi, Heat transfer in compression chamber of a revolving vane (rv) compressor, Applied Thermal Engineering 31 (89) (2011) 1519 – 1526. doi:10.1016/j.applthermaleng.2011.01.041.

[27] M. Fowell, S. Medina, A. Olver, H. Spikes, I. Pegg, Parametric study of texturing in convergent bearings, Tribology International 52 (2012) 7 – 16. doi:10.1016/j.triboint.2012.02.013.

[Table 4 about here.]

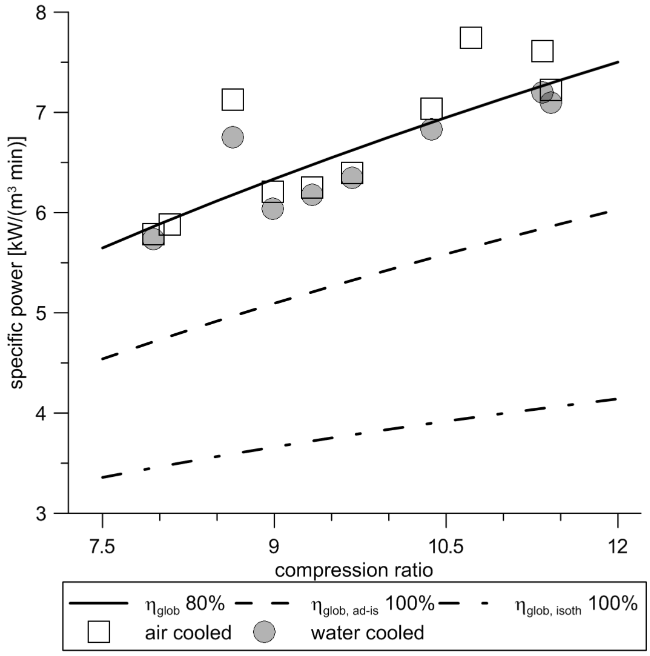

Figure 1: Energy saving potential in industrial rotary compressors: comparison between best available technologies and ideal performances (elaborations from CAGI datasheets [4])

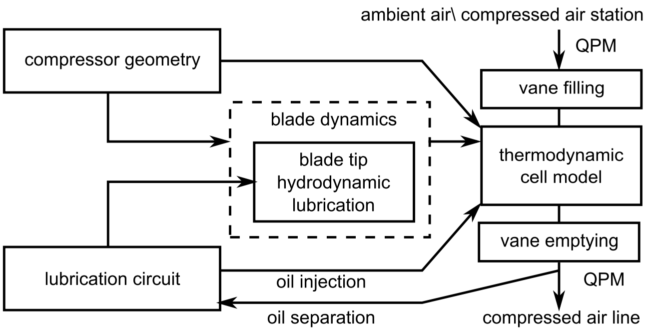

Figure 2: Block diagram of the comprehensive compressor model

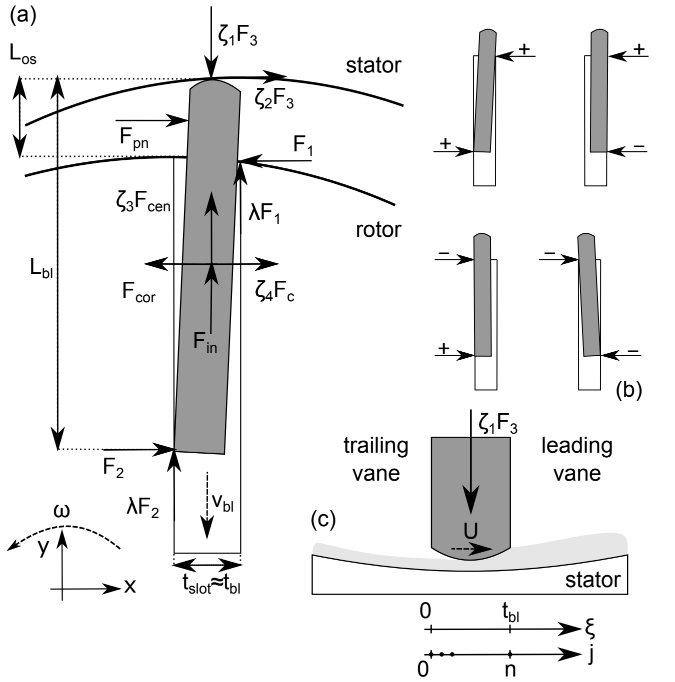

Figure 3: Free body diagram of the compressor blade (a), possible arrangements (b), hydrodynamic lubrication at the blade tip (c)

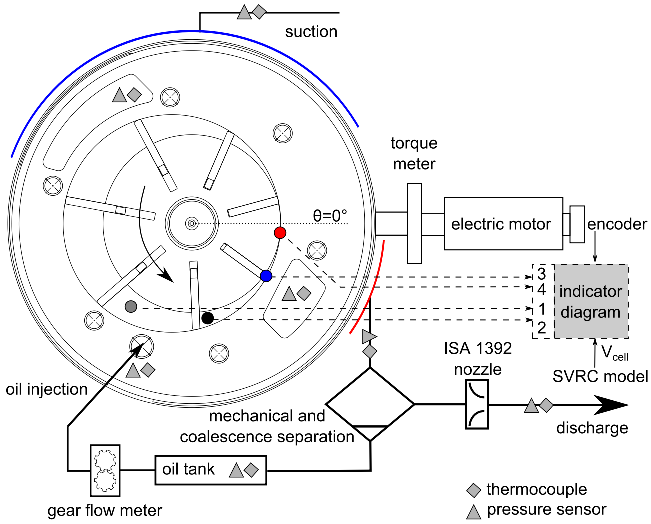

Figure 4: Experimental setup

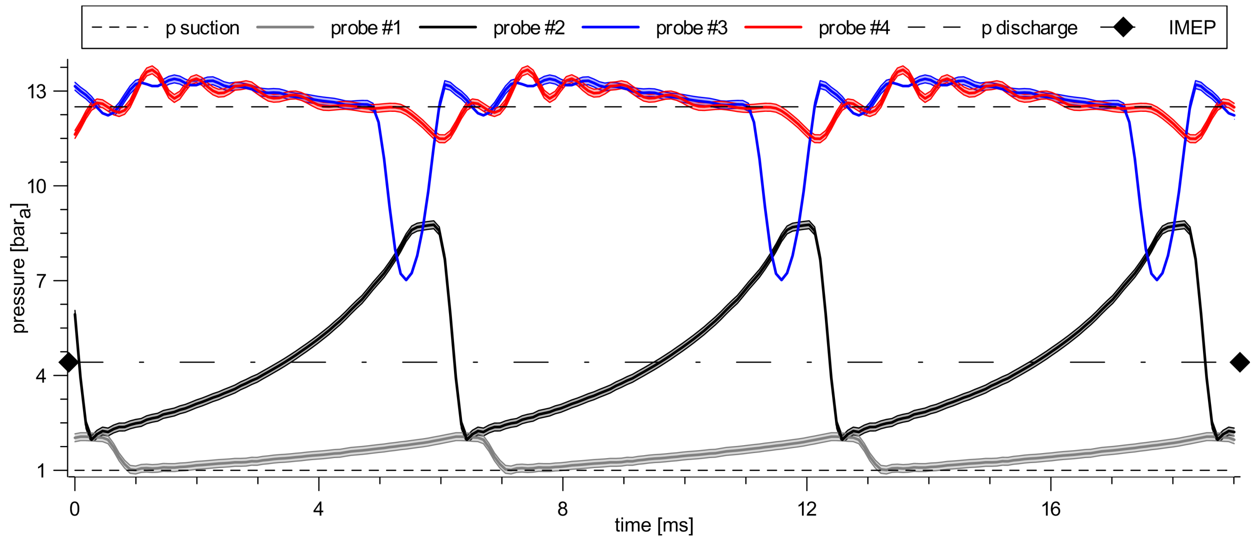

Figure 5: Ensemble averaged data from the high-frequency transducers with uncertainty bands and pressure offsets applied to match the suction and discharge pressures (test at 1500 RPM and 12.5 bar)

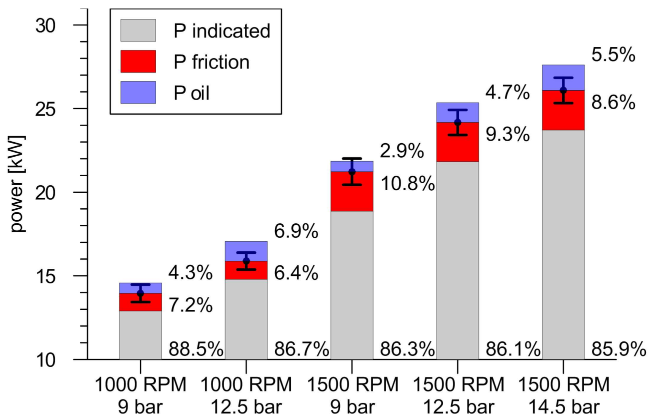

Figure 6: Compressor energy balance at different operating points (percentages refer to the mechanical power)

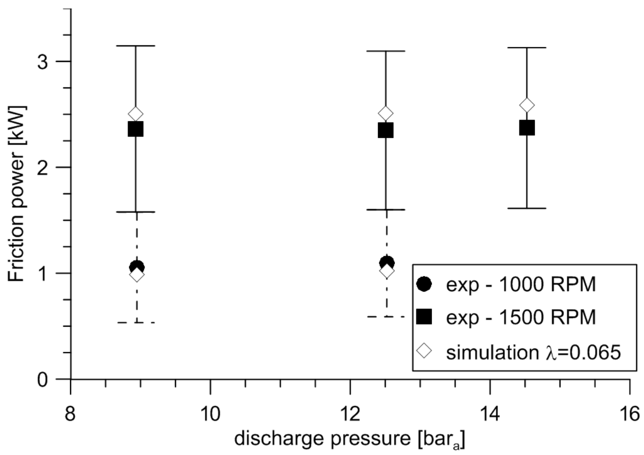

Figure 7: Experimental and simulated evaluations of the friction power that identified the friction coefficient λ

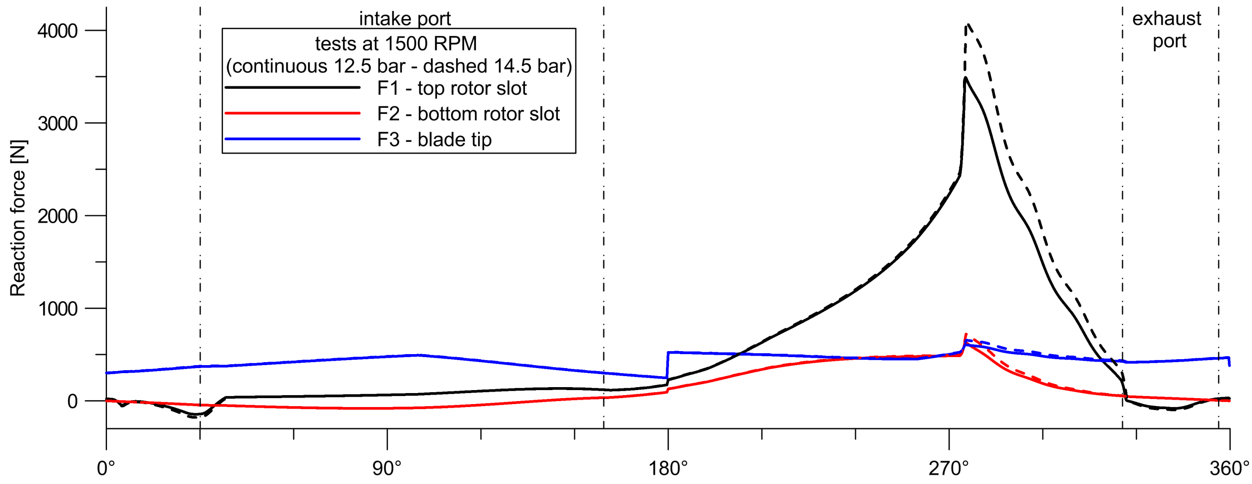

Figure 8: Reaction forces at the friction locations at different discharge pressures (λ=0.065)

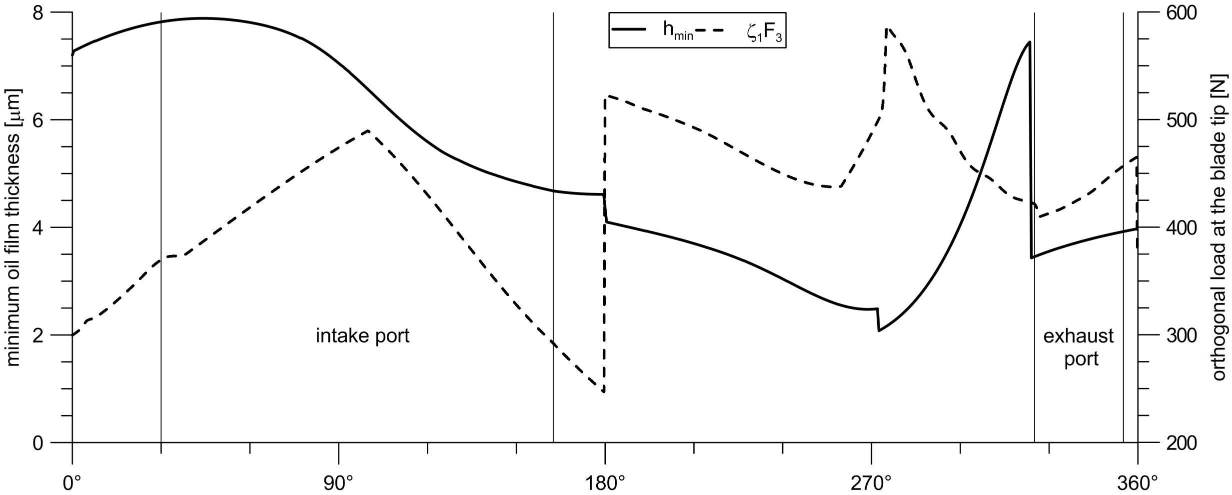

Figure 9: Oil film thickness evolution and normal load at the blade tip (test at 1500 RPM, 12.5 bar)

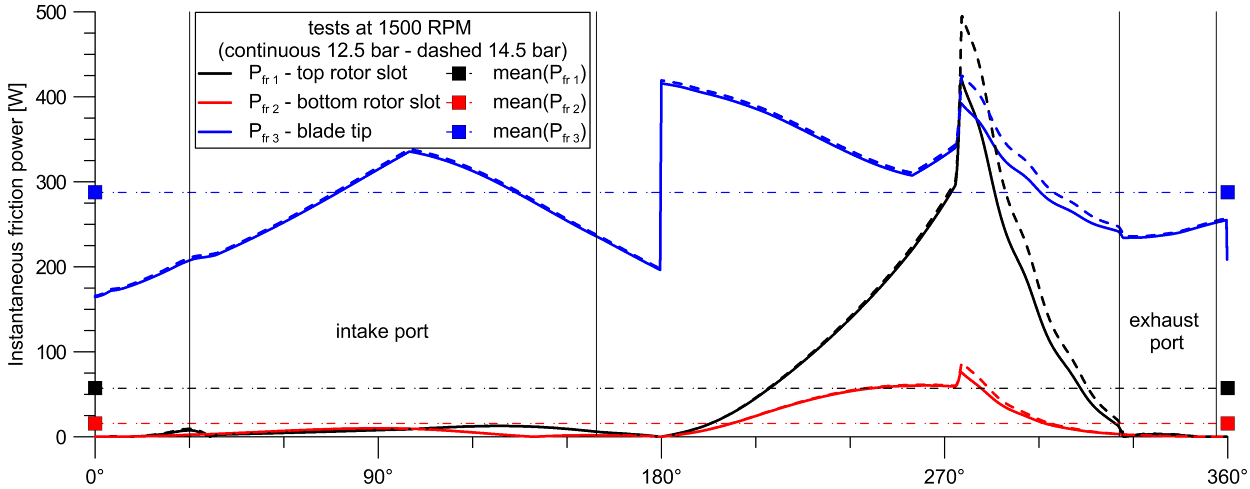

Figure 10: Friction power decomposition (λ=0.065)

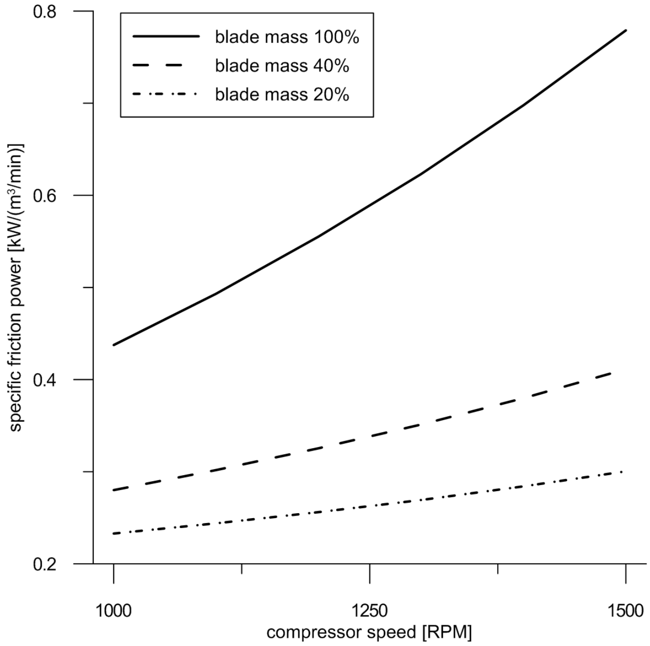

Figure 11: Effects of blade mass and revolution speed on the specific friction losses (compressor of Table 1 operating at 12.5 bar)

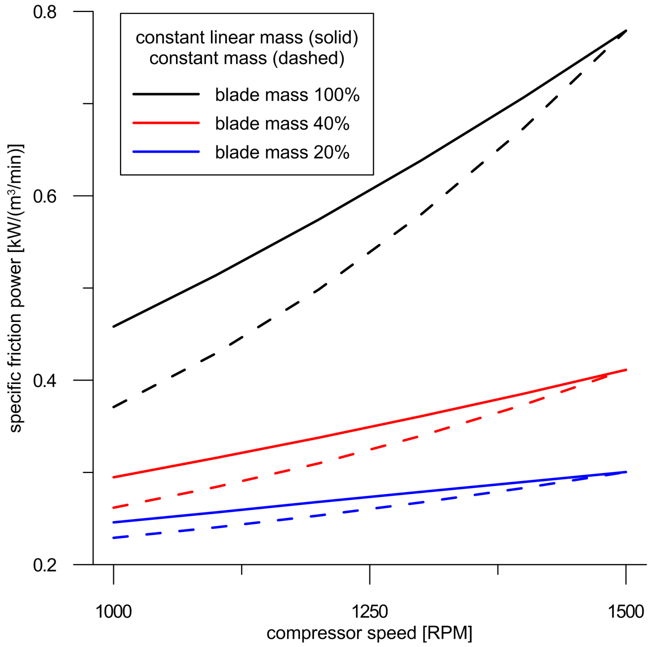

Figure 12: Effects of the combined variation of compressor aspect ratio and revolution speed on the specific friction power - simulations performed with constant linear mass and constant mass approaches at 12.5 bar as outlet pressure

stator diameter	$136\,mm$	Intake port start	$30°$
rotor diameter	$111\,mm$	Intake port end	$162°$
axial length	$275\,mm$	Exhaust port start	$325°$
number of cells	7	Exhaust port end	$356°$

Table 1: Geometrical features of the compressor tested (Mattei ERC 22 L)

$\Delta\, C$	$\Delta\, \omega$	$\Delta\, Q_{oil}$	$\Delta\, p_{tank}$	$\Delta\, p(\theta_{inj})$
0.2 N m	1 RPM	1 L/min	0.03 bar	0.03 bar

Table 2: Direct measurements uncertainties

p_{outlet}	bar_a	8.9	12.5	8.9	12.5	14.5
ω	RPM	995	981	1470	1451	1455
C	$N\,m$	140.0	166.0	142.0	167.0	181.2
Q_{oil}	L/min	44	56	43	55	60
p_{tank}	bar_a	8.82	12.33	8.74	12.29	14.33
$p(\theta_{inj})$	bar_a	1.30	1.31	1.23	1.24	1.22
P_{mech}	kW	14.6	17.1	21.9	25.4	27.6
Q_{air}	m^3/min	3.03	3.09	4.24	4.26	4.14
$IMEP$	bar_a	3.95	4.43	3.92	4.42	4.71
ΔP_{ind}	%	4.2	3.6	4.3	3.7	3.4
ΔP_{fr}	%	49.5	46.2	33.2	31.9	32.0

Table 3: Summary of the experimental campaign

List of Symbols

h	oil film thickness	$[\mu m]$
k	specific heat ratio	$[-]$
q	oil flow rate per unit surface	$[m/s]$
t	thickness	$[m]$
u	oil flow velocity	$[m/s]$
v	sliding blade speed	$[m/s]$
C	torque	$[N\,m]$
E	specific energy consumption	$[kW/(m^3\,min)]$
F	force	$[N]$
L	length	$[m]$
N	number of cells	$[-]$
P	power	$[W]$
Q	flow rate	$[L/min]$
R	air gas constant	$[J/kg/K]$
T	temperature	$[K]$
P	blade tip speed	$[m/s]$
V	volume	$[m^3]$
β	manometric compression ratio	$[-]$
η	efficiency	$[rad]$
θ	angle	$[rad]$
λ	friction coefficient	$[-]$
μ	oil dynamic viscosity	$[Pa \cdot s]$
ζ	projection coefficient	$[-]$
ω	revolution speed	$[rad/s]$

Subscripts

0	film thickness at maximum pressure
$ad-is$	adiabatic-isentropic
bl	blade
cen	centrifugal
cor	Coriolis
el	electrical
$glob$	global
fr	friction
in	inertia
ind	indicated
inj	injection
inl	inlet
$isoth$	isothermal
$mech$	mechanical
oil	inlet
org	organic
os	outside the rotor slot
pn	normal pressure
vol	volumetric

Acronyms

$IMEP$	indicated mean effective pressure
LV	leading vane
$SVRC$	sliding vane rotary compressor
TV	trailing vane